ACS APPLIED MATERIALS & INTERFACES

Research Article

www.acsami.org

Metal–Organic–Inorganic Nanocomposite Thermal Interface Materials with Ultralow Thermal Resistances

Cengiz Yegin,[†] Nirup Nagabandi,[‡] Xuhui Feng,[§] Charles King,[§] Massimo Catalano,[∥,⊥] Jun Kyun Oh,[†] Ansam J. Talib,[#] Ethan A. Scholar,[‡] Stanislav V. Verkhoturov,[&] Tahir Cagin,[†,‡] Alexei V. Sokolov,[#] Moon J. Kim,[⊥] Kaiser Matin,[%] Sreekant Narumanchi,[§] and Mustafa Akbulut*[,†,‡]

[†]Department of Materials Science and Engineering, Texas A&M University, 3003 TAMU, College Station, Texas 77843-3003, United States

[‡]Artie McFerrin Department of Chemical Engineering, Texas A&M University, 3122 TAMU, College Station, Texas 77843-3122, United States

[§]National Renewable Energy Laboratory (NREL), 15013 Denver West Parkway, Golden, Colorado 80401, United States

[∥]CNR-IMM, Institute Microelectronics and Microsystems, National Council for Research, Via Monteroni, 73100 Lecce, Italy

[⊥]Materials Science and Engineering Department, University of Texas at Dallas, 800 W. Campbell Rd., Richardson, Texas 75080, United States

[#]Department of Physics and Astronomy and Institute for Quantum Science and Engineering, Texas A&M University, 4242 TAMU, College Station, Texas 77843-4242, United States

[&]Department of Chemistry, Texas A&M University, 3012 TAMU, College Station, Texas 77843-3012, United States

[%]Microsystems Technology Office, Defense Advanced Research Project Agency, 675 N Randolph St., Arlington, Virginia 22203, United States

Supporting Information

ABSTRACT: As electronic devices get smaller and more powerful, energy density of energy storage devices increases continuously, and moving components of machinery operate at higher speeds, the need for better thermal management strategies is becoming increasingly important. The removal of heat dissipated during the operation of electronic, electrochemical, and mechanical devices is facilitated by high-performance thermal interface materials (TIMs) which are utilized to couple devices to heat sinks. Herein, we report a new class of TIMs involving the chemical integration of boron nitride nanosheets (BNNS), soft organic linkers, and a copper matrix—which are prepared by the chemisorption-coupled electrodeposition approach. These hybrid nanocomposites demonstrate bulk thermal conductivities ranging from 211 to 277 W/(m K), which are very high considering their relatively low elastic modulus values on the order of 21.2–28.5 GPa. The synergistic combination of these properties led to the ultralow total thermal resistivity values in the range of 0.38–0.56 mm^2 K/W for a typical bond-line thickness of 30–50 μm, advancing the current state-of-art transformatively. Moreover, its coefficient of thermal expansion (CTE) is 11 ppm/K, forming a mediation zone with a low thermally induced axial stress due to its close proximity to the CTE of most coupling surfaces needing thermal management.

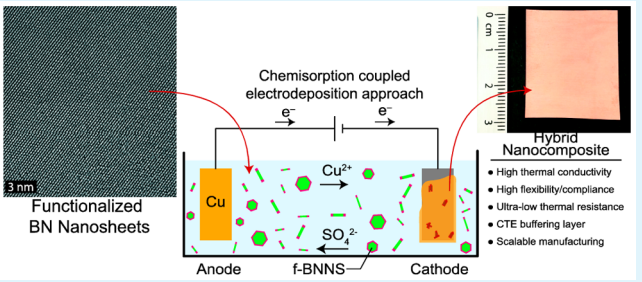

KEYWORDS: *thermal management, thermal interface materials, boron nitride nanosheets, hybrid nanocomposites, nanostructures, nanomaterials, thermal conductivity*

1. INTRODUCTION

The removal of heat dissipated during the high power density operations is typically achieved by the transfer of heat by conduction from a heat source to a heat sink.[1,2] When these two surfaces are brought together in the absence of any TIM, surface roughness—which all engineered objects have—causes the thermal contact to occur only at discrete junctions.[3,4] The resultant thermal contact is characterized by nano- and microjunctions surrounded with a large volume fraction of interstitial air or pores. Such pores reduce the effective thermal conductivity of the contact region, often termed as the thermal contact resistance. In addition, the heat transfer across the

Received: January 4, 2017
Accepted: February 27, 2017
Published: February 27, 2017

DOI: 10.1021/acsami.7b00093
ACS Appl. Mater. Interfaces XXXX, XXX, XXX–XXX

contact junctions is further reduced owing to the thermal boundary resistance stemming from phonon or electron scattering processes depending on the nature of materials comprising the interface.[5] Moreover, when the size of contact junctions becomes comparable with the mean free path of the energy carriers, their transport is further hindered through the quantum confinement effect and changes in phonon/electron dispersion.[6] One potential approach for overcoming these problems is to use TIMs that enable a better thermal contact by conforming to the topographical features of the coupling surfaces via flow or deformation without introducing a significant conductive resistance into the system and by reducing the sharp acoustic mismatch between air and solid surfaces.

Currently, thermal greases, polymer composites, and solders are the most commonly used types of TIMs. In thermal greases, thermally conductive fillers are dispersed in a viscous fluid such as silicone oil, sodium silicate, or hydrocarbon oil to form a paste.[7] In polymer-composite TIMs, the matrix is a macromolecule instead of a viscous fluid, such as epoxy or polyurethane.[8,9] In both types of TIMs, a high thermal conductivity material such as graphene, carbon nanotubes, diamond powder, silver particles, and copper particles is used as a filler.[3,10−18] Thermal grease and polymer-composite TIMs typically have bulk thermal conductivity values in the range of 0.5−10 W/(m K) at room temperature.[19] These TIMs are compliant and reusable, but their low thermal conductivity and poor thermal transport across the boundaries pose a significant thermal barrier to high power-density operations. In addition, these TIMs also suffer from pump-out and dry-out issues when subjected to thermal cycling and elevated temperatures, which degrades their performance. Solder TIMs, which are fusible metal alloys with low melting temperatures, have a thermal conductivity of 20−80 W/(m K).[19,20] While solder TIMs offer relatively high thermal conductivities, solder TIMs—similar to other low-melting-temperature metals—tend to have a high coefficient of thermal expansion (CTE). For instance, the CTE of indium is 29 ppm/K while the CTE of silicon and copper is 2.4 and 16.4 ppm/K, respectively,[21] making them prone to thermally induced high-stress failure. For a typical bond line thickness of 50 μm, the total thermal resistance is on the order of 5−30 mm^2 K/W for thermal greases, polymer TIMs, and solders TIMs.[22] Another important type of TIM is highly oriented pyrolytic graphite, which has very high thermal conductivity along the in-plane direction (600−1700 W/(m K)) and low thermal conductivity in the out-of-plane direction (10−20 W/(m K)).[23,24] However, most thermal management applications require a high thermal conductivity in the out-of-plane (z) direction between heat spreader and sink. While graphene-based TIMs achieved thermal resistances as low as 1.5 × 10^{-2} mm^2 K/W at the nanoscale,[25,26] their device scale forms and highly oriented pyrolytic graphite sheets with a thickness of 50−100 μm have been reported to result in a total resistance on the order of 20 mm^2 K/W.[27] The delamination and flaking off are other challenges associated with pyrolytic graphite sheets.

There are two potential routes for reducing the total thermal resistance of TIMs that are needed to satisfy stringent thermal needs of emerging advanced applications: either by further improving the thermal properties of a compliant matrix or by further improving the mechanical properties of a high-thermal-conductivity matrix. Currently, the majority of research is focused on the former approach. As ours is a novel approach aiming at the enhancement of the mechanical properties of the metal matrix, we develop a new class of nanocomposite TIMs by covalently integrating boron nitride nanosheets (BNNS) functionalized with soft organic linkers and a copper matrix. Here, BNNS is selected as filler because of its extremely high in-plane thermal conductivity (300−1000 W/(m K)), low coefficient of thermal expansion, and superior thermal and chemical stability.[28−31] Copper is a well-known matrix material with high thermal conductivity. A few recent works related to our approach are silver coated onto polyimide network in an indium matrix,[32] matrix silver coated on to a polymer mesh in a Sn−Ag−Cu alloy matrix,[33] BN−In TIMs made from boron nitride nanofibers and indium,[34] and carbon fiber-based tin−silver−copper alloy matrix composite.[35] However, none of these approaches rely on the chemical linking of metal matrix and filler, the lack of which results in an increased thermal boundary resistance and phonon scattering as evidenced by the observed thermal resistances above 2 mm^2 K/W in these studies.

2. EXPERIMENTAL SECTION

2.1. Materials. Hexagonal boron nitride, h-BN (98%, APS: 0.5 μm), produced by the reaction of boric acid and ammonia at 900 °C ($B(OH)_3 + NH_3 \rightarrow BN + 3H_2O$) was received from Lower Friction-M.K. IMPEX Corp, (Mississauga, Ontario, Canada). Sulfuric acid (H_2SO_4, ACS reagent, 95.0−98.0%), copper(II) chloride ($CuCl_2$, 99%), and copper sulfate pentahydrate ($CuSO_4{\cdot}5H_2O$, ≥98%) were obtained from Sigma-Aldrich (St. Louis, MO). Thiosemicarbazide (CH_5N_3S, >98%) and 1,3,4-thiadiazole-2,5-dithiol ($C_2H_2N_2S_3$, >95%) were obtained from TCI America (Portland, OR). *N*-Methlyl-2-pyrrolidone (C_5H_9NO, 99%) (NMP) was obtained from VWR (Radnor, PA). Copper sheets were obtained from McMaster Carr (Elmhurst, IL), and aluminum substrate was obtained from Metals Depot (Winchester, KY). Silicon wafers (silicon ⟨100⟩ P/boron, >5000 ohm·cm, double-side polish, <10 Å R_a) were received from University Wafer (Boston, MA).

2.2. Functionalization of BNNS. Covalent functionalization of BNNS was achieved by reacting exfoliated BNNS with thiosemicarbazide (>98%) in NMP (1:10:100 in weight). The reaction took place at 170 °C for 30 h under nitrogen flow. The obtained product was dialyzed in NMP for 10 h to remove the unreacted ligands, followed by centrifugation at 3500 rpm for 15 min. Next, the supernatant was removed, and the precipitate (functionalized BNNS, f-BNNS) was dried at 75 °C in a vacuum furnace for further removal of the remaining NMP from f-BNNS powder.

2.3. Chemical and Structural Analysis of f-BNNS. Nuclear magnetic resonance spectra in solid state were obtained on an AVANCE-400 instrument. ^{11}B shifts are reported relative to $BF_3(OEt_2)$. High-power proton decoupling was applied with a 90° pulse time of 5 μs, a contact time of 5 ms, and a recycle delay of 8 s. Approximately 50 mg of the sample was packed into 5 mm Wilmad thin wall precision NMR sample tube 8 in. and loaded in to 7 mm CP-MAS rotors. The rotor spinning speeds were 4 kHz. All NMR measurements were carried out at 25 °C. Transmission electron microscopy was performed in a JOEL ARM200F electron microscope operated at 200 kV, with spherical aberration (Cs) corrector, also equipped with an Oxford Instruments X-MaxN 100TLE 100 mm^2 detector for energy dispersive X-ray spectroscopy (EDS) and a Gatan Enfina spectrometer for electron energy loss spectroscopy (EELS). High angle annular dark field (HAADF) and annular bright field (ABF) scanning transmission electron microscopy (STEM) imaging techniques were used to characterize the nanostructural morphology of the BNNS samples.

2.4. Fabrication of Nanocomposite TIMs. Nanocomposite TIMs were grown on aluminum sheets and silicon substrates. The aqueous electrolyte solutions were prepared by varying concentrations of $CuSO_4{\cdot}5H_2O$, 1.8 M H_2SO_4, a trace amount of $CuCl_2$, and various concentrations of f-BNNS. Each solution was briefly sonicated for

DOI: 10.1021/acsami.7b00093
ACS Appl. Mater. Interfaces XXXX, XXX, XXX−XXX

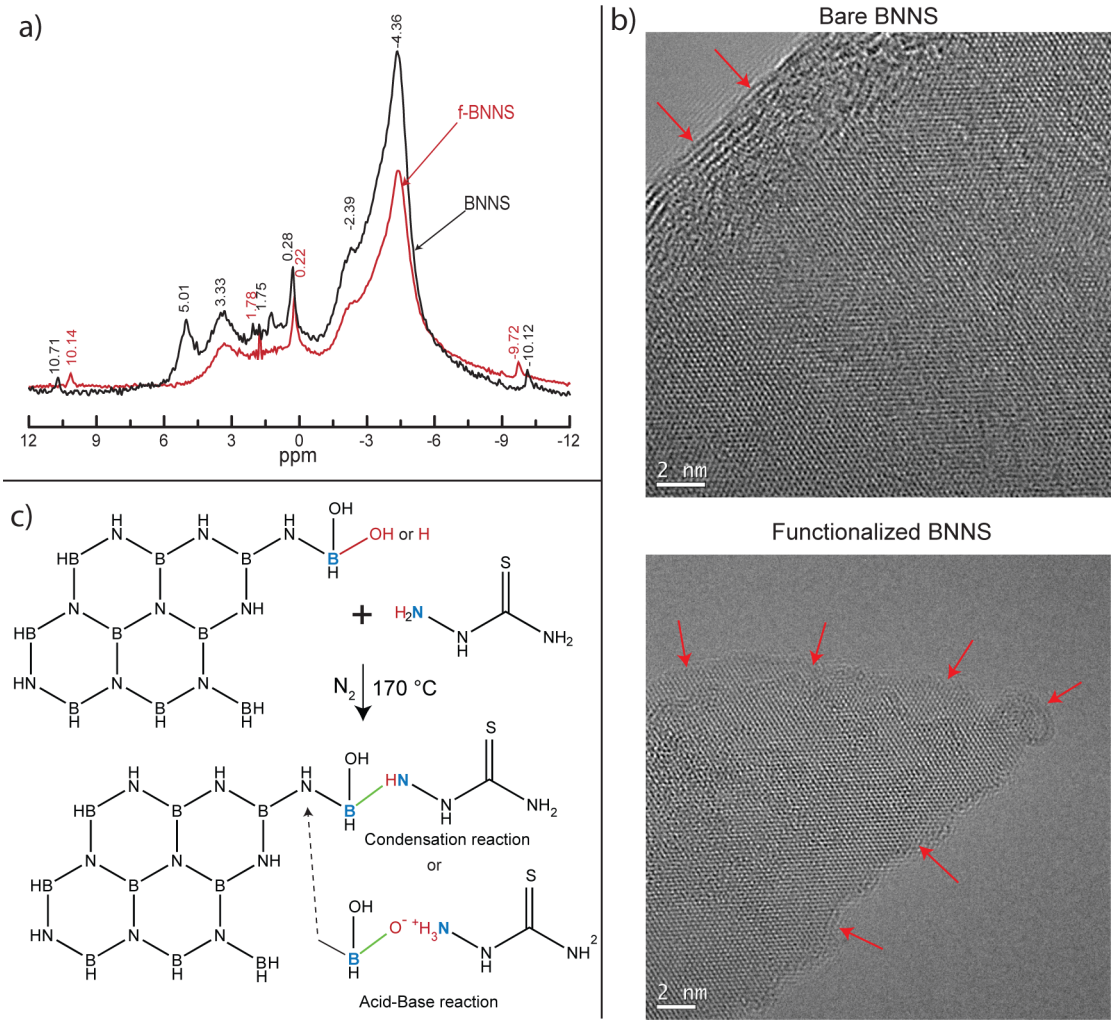

Figure 1. (a) ^{1}H MAS NMR spectra of BNNS before and after the functionalization reaction with thiosemicarbazide, (b) HR-TEM micrographs of BNNS before and after the functionalization reaction, and (c) proposed reaction schemes.

homogeneous dispersion of f-BNNS and transferred to an electroplating cell. A pure copper sheet (>99%) and a substrate were connected to the anode and cathode, respectively. The electrical power source was a Nuvant Powerstat05 potentiostat (Nuvant Systems Inc., Crown Point, IN). The electrodeposition was carried out at a current density of 0−12 A/dm^2 and alternating current (AC) frequency of 950 Hz with 30% off time. The main advantage of the pulse electrodeposition is the ability to change experimental parameters such as pulse peak current density and on/off time in pulse electrodeposition. Manipulation of these parameters enabled us to better control the homogeneity of nanocomposite TIMs.

2.5. Characterization of Mechanical Properties. Reduced elastic modulus values were measured via a Hysitron TI 950 triboindenter (Hysitron Inc., Minneapolis, MN). A Berkovich tip with a well-defined geometry was used for indentation, and 40 measurements were taken from each sample for statistical analysis. The reduced modulus values were later converted to Young's modulus via the Poisson's ratio as described elsewhere.[36]

2.6. Characterization of Thermal Properties. A modulated Q20 DSC (TA Instruments, New Castle, DE) was used to measure specific heat capacity, c_p, of the samples. Thermal diffusivity measurements were performed via a DLF-1200 laser flash diffusivity system (TA Instruments, New Castle, DE). The density, ρ, of samples was determined gravimetrically. Thermal conductivity, κ, of samples was calculated using the measured thermal diffusivity (α), specific heat capacity (c_p), and density (ρ) values as follows:

$$\kappa = \alpha \rho c_p \quad (1)$$

Further, phase-sensitive transient thermoreflectance (PSTTR) measurements were done at NREL, Colorado, to compare the thermal conductivity values obtained through DLF and to determine the contact and total thermal resistances of the samples (see Supporting Information for further details).

Further details and extended versions of the experimental methods are given in the Supporting Information.

3. RESULTS AND DISCUSSION

3.1. Functionalization of BNNS with Thiosemicarbazide. The first step in producing metal/organic/inorganic nanocomposite TIMs was the functionalization of the boron nitride nanosheets with a ligand that is capable of reducing their effective stiffness and covalently linking BNNS with the metal matrix. Towards this end, we relied on thiosemicarbazide (TSC), which contains an amino group that can react with electron deficient boron groups of BNNS, and a carbonothioyl group (or its tautomer, thiol) that can react with copper. To gain insights into the reaction of TSC with BNNS, first, solid state ^{1}H MAS (magic-angle spinning) NMR (nuclear magnetic resonance) was used (Figure 1a). The major changes were observed as disappearance of peak at δ = 5.01; this is hydrogen in the hydroxyl group on an edge B atom. This indicates reaction with TSC as a condensation reaction. This was also

DOI: 10.1021/acsami.7b00093
ACS Appl. Mater. Interfaces XXXX, XXX, XXX−XXX

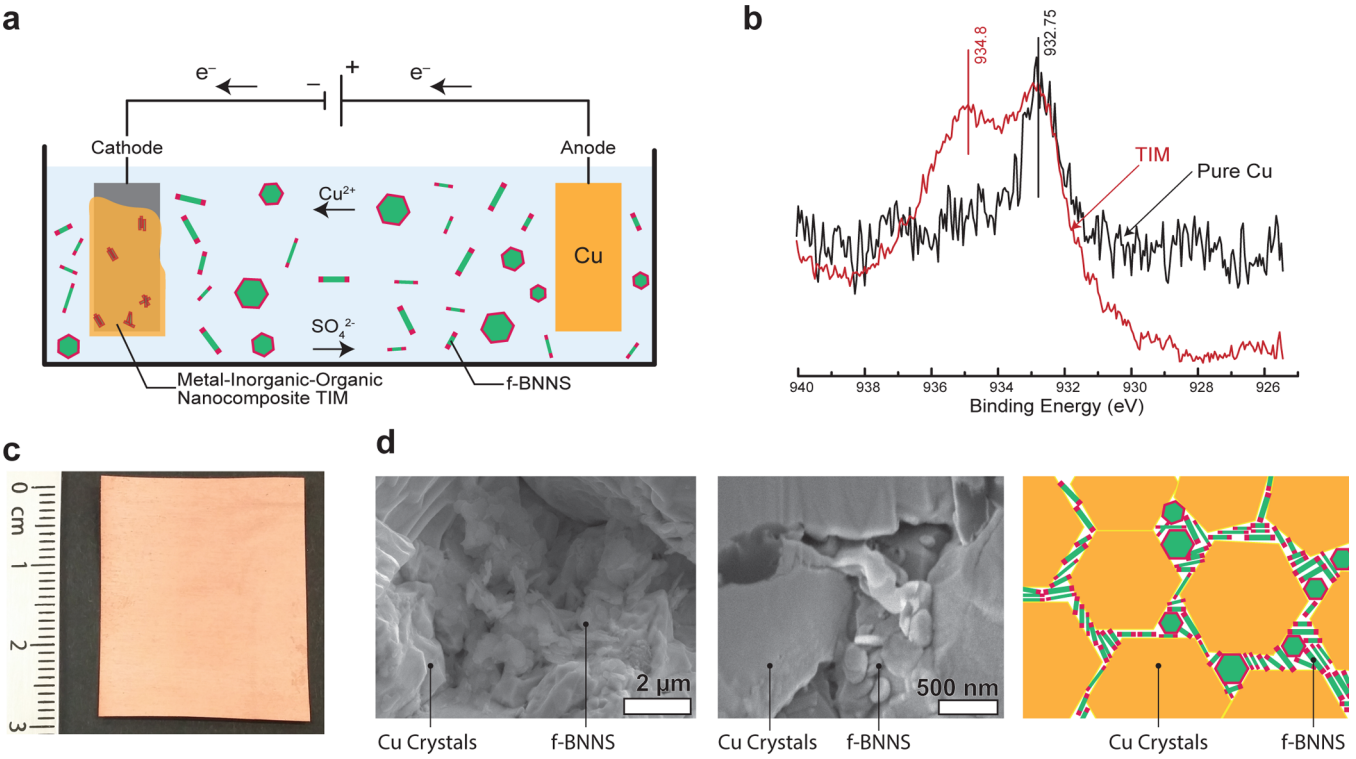

Figure 2. (a) Illustration of the chemisorption coupled electrodeposition approach, (b) XPS analysis of copper in pure copper and nanocomposite TIM, (c) photograph of a typical metal/organic/inorganic nanocomposite TIM, and (d) SEM micrographs and schematic illustration showing the distribution of f-BNNS across the copper matrix.

supported by ^{11}B MAS NMR spectrum for BNNS and f-BNNS shown in Figure S3. No change was observed in basal B atoms at δ = 20.8, but prominent change was recorded on tetracoordinated B atoms at δ = −25.7 to −17.2, indicating the site of reaction. Further studies with Raman spectroscopy revealed the disappearance and major shifts at wavelengths 806 cm^{-1} (NH_2 wagging and CS stretching), 1008 cm^{-1} (NN stretching and CN stretching), 1172 cm^{-1} (NN stretching), 1526 cm^{-1} (NH bending), 1630 cm^{-1} (NH_2 bending), and 3258 cm^{-1} (NH_2 stretching) from the TSC spectra upon the reaction with BNNS (Figure S4). These findings demonstrate that the most notable changes on TSC occur on the amino group. On the other hand, no significant change in the peaks associated with the primary amide was observed (see Supporting Information for details), proving that the functionalization reaction indeed takes place between the amino group of TSC and BNNS.

The comparison of high-resolution TEM micrographs of BNNS before and after the functionalization step revealed that the functionalization occurs at the edges rather than on the basal plane (Figure 1b), which is preferred in 2-D materials to prevent the loss of intriguing properties. The complementary X-ray photoelectron spectroscopy (XPS) studies showed that some fraction of carbonothioyl was converted to tautomeric thiol upon the functionalization reaction (Figure S2). When we put all of these pieces together, the picture emerges that the electron-rich amino group of TSC reacts with hydroxylated and tetracoordinated boron atoms of BNNS via either condensation or Lewis acid−base reaction (Figure 1c). In this reaction scheme, the carbonothioyl (or its tautomer, thiol) group sticking out of the f-BNNS is available for coordination bonding with copper.

3.2. Formation of Nanocomposites via Chemisorption-Coupled Electrodeposition. Traditional molten metal-based mixing and agitation approaches for metal/inorganic nanocomposites are not feasible for producing metal/inorganic/organic hybrid nanocomposite TIMs due to the presence of organic linker molecules and the high melting temperature of copper. To overcome this challenge, we developed a programmed electro-codeposition approach by which the reduction of copper ions and the nucleation and growth of the resultant elemental copper on the cathode occurs, while f-BNNS experiences Brownian motion and reaches the cathode through diffusion (Figure 2a). Once the f-BNNS-bearing carbonothioyl/thiol groups on the terminal edges come into the contact with copper crystals, the chemisorption reaction takes place (Figure 2b). The coordination reaction between copper atom and sulfurous groups was confirmed through X-ray photoelectron spectroscopy (XPS) studies as evidenced by a shift in binding energy of some fraction of copper from 932.75 to 934.80 eV. The interplay among these three processes determines the nanostructure of the resultant metal/inorganic/organic hybrid nanocomposite. It is also possible to manipulate the nanostructure by adjusting the composition and pH of electrolyte, current density, and temperature. Using this approach, we were able to produce fairly homogeneous films (Figure 2c). The fracture SEM studies revealed that the nanocomposite TIMs developed have a peculiar nanostructure in that f-BNNS are localized only at the grain boundaries of copper crystals (Figure 2d), the manifestation of which on the mechanical and thermal properties will be discussed in the subsequent paragraphs.

3.3. Thermal Properties of Nanocomposite Thermal Interface Materials. The bulk thermal conductivity of the nanocomposite TIM, measured via the laser flash diffusion

DOI: 10.1021/acsami.7b00093
ACS Appl. Mater. Interfaces XXXX, XXX, XXX−XXX

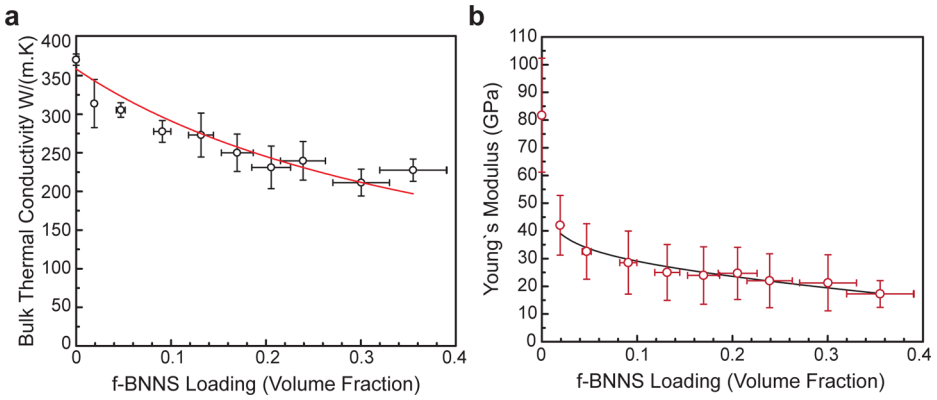

Figure 3. (a) Variation in the bulk thermal conductivity of the hybrid nanocomposite TIM as a function of functionalized boron nitride nanosheet (f-BNNS) loading. The fit is based on the percolation theory. (b) Influence of f-BNNS content on the Young's modulus of the hybrid nanocomposite. The fitted line is obtained through the modified Halpin−Tsai model with discontinuous fillers. Error bars represent one standard deviation in both cases.

technique as well as the phase-sensitive transient thermoreflectance technique, was found to decrease with increasing amount of f-BNNS in the copper matrix, with diminishing returns (Figure 3a). The reductions due to the presence of organic linker molecules was relatively low (up to 40%, from 370 to 211 W/(m K)), which is ascribed to the fact that TSC covalently attaches BNNS to copper matrix. This is consistent with the findings of Losego et al.[37] showing that the strength of a single bonding layer directly governs phonon heat transport across an interface. Strong covalent interactions lead to much higher interfacial thermal conductance in comparison to the weak van der Waals interactions due to ability to form an effective gradient for reducing the impedance mismatch. Furthermore, the localization of TSC at the edges of BN nanosheets can guide phonons through the in-plane direction along nanosheets rather than the out-of-plane direction, along which the thermal conductivity of 2-D materials is about 2 orders of magnitude lower than that in the in-plane direction.

The details of complex thermal transport across the metal/inorganic/organic nanocomposite can be explained with a combination of phononic and electronic modes. In the absence of f-BNNS, the system is in a percolated regime with interconnected copper microcrystals where the thermal transport is mostly through electrons. As f-BNNS is introduced into the system, while the degree of percolation of copper microcrystals decreases, new phonon bandwidth emerges via f-BNNS linkers owing to anharmonic phonon−phonon coupling and electron−phonon coupling at the metal−linker interface.[38] Overall, organic linkers, filtering some phonon modes as well as scattering moieties for electron transport, act as a bottleneck to thermal transport and result in a reduction of thermal conductivity of pure BNNS and thus the overall composite. Bulk thermal conductivities of copper matrix and f-BNNS calculated according to fit explained by Phelan et al.[39] were 370 and 100 W/(m K), respectively, which are in agreement with recent studies.[40] Introduction of f-BNNS in copper grain boundaries replaces a part of electronic thermal transport with phonon thermal transport. As f-BNNS loading is increased, more such sites reduce the thermal conductivity until no new sites are occupied by f-BNNS. We see this region is obtained around the 0.12 volume fraction (Figure 3a), and beyond this point, no more reduction in thermal conductivity is observed.

The coefficient of thermal expansion (CTE) of the hybrid nanocomposite was measured to be 11 ppm/K, while that of pure silicon and pure copper, which are two common heat source/sink pairs, are 2.4 and 16.4 ppm/K, respectively.[21] The compatibility of CTE of TIMs with the coupling surfaces plays a vital role in relieving mechanical stresses arising from the CTE mismatch at the interface during thermal cycling.[41] Given that the CTE of solder and polymer TIMs are in the range of 25−90 and 20−50 ppm/K, respectively,[42,43] the close proximity to CTE of common metals and semiconductors relying on TIMs is another advantage of the hybrid nanocomposites.

3.4. Mechanical Properties of Nanocomposite Thermal Interface Materials. When a heat source and a heat sink are coupled through a TIM, the asperities of heat source/sink surface apply compressive stress in the perpendicular direction to the TIMs. Thus, a nanoindentation technique, involving a very similar geometry, is used as the main mechanical characterization technique in this study. As shown in Figure 3b, the Young's modulus of the hybrid nanocomposite gradually decreased with the increasing f-BNNS content in the hybrid nanocomposite, slowly plateauing around 20 GPa. This trend can be attributed to the interplay among metallic bonds between copper atoms; van der Waals interactions between copper microcrystals, between copper microcrystals and BNNS, and between BNNS; the bond strengths of ligand−BNNS pair and ligand−copper microcrystal pair; and buckling or bending of BNNS. In the absence of f-BNNS, the mechanical properties of copper are determined by van der Waals forces and metallic bonds holding copper microcrystals together. When f-BNNS is introduced to the matrix, the van der Waals forces between copper microcrystals decrease due to the screening effects induced by the presence of less polarizable materials and the increased distance between microcrystals, which also causes the disappearance of the short-ranged intercrystalline metallic bonds.[44] However, new forces stemming from the linking of copper to BNNS through thiol/copper and amine/BNNS bonds also arise. Because f-BNNS is only functionalized from the edges, the latter effect cannot balance the former effect, resulting in a reduction in the Young's modulus. As the f-BNNS loading increases, the formation of f-BNNS aggregates between grain boundaries occurs. Considering that van der Waals interactions between metals are much higher than that between inorganics or organics, the presence of f-BNNS aggregates, in turn,

DOI: 10.1021/acsami.7b00093
ACS Appl. Mater. Interfaces XXXX, XXX, XXX−XXX

introduces regions that are held together through weak van der Waals forces in the nanocomposite.

The modulus values were also obtained from the modified Halpin–Tsai model by considering the f-BNNS as randomly oriented discontinuous fillers:[45,46]

$$E_c = \left[\frac{3}{8}\frac{1 + 2(l_f/d_f)\mu_L v_f}{1 - \mu_L v_f} + \frac{5}{8}\frac{1 + 2\mu_T v_f}{1 - \mu_T v_f}\right]E_M \quad (2)$$

where $\mu_L = \frac{(E_f/E_M) - 1}{(E_f/E_M) + 2(l_f/d_f)}$, $\mu_T = \frac{(E_f/E_M) - 1}{(E_f/E_M) + 2}$, E_c, E_M, and E_f are the elastic moduli of the composite, matrix, and filler, respectively, and l_f, d_f, and v_f are the filler thickness, diameter, and volume fraction, respectively. The calculations from the model yielded the elastic moduli of copper and the f-BNNS to be 48.2 and 1.6 GPa, respectively (r^2 = 0.952). The resultant elastic modulus of pure copper was somewhat lower than the literature value, which is well-known to occur for electrodeposited materials due to the formation of nano- and micropores.[47,48] Most organic ligands have elastic moduli less than 1 GPa,[49] and the reported out-of-plane bending and in-plane elastic modulus of BNNS are 20–30 GPa[50] and 0.8–1.2 TPa,[51] respectively. In addition, the organic ligands constitute a small fraction of f-BNNS volume (1.4%–1.2%) due to the functionalization only on the edges. Hence, an effective modulus of 1.6 GPa for the filler implies that f-BNNS behaves closer to the Reuss model (the lower-bound modulus) where the elastic modulus is averaged via the inverse rule of mixtures.

3.5. Thermal Resistivity Measurements. PSTTR measurements revealed that the combination of these thermal and mechanical properties gave rise to a total thermal resistance of 0.38 ± 0.10 mm^2 K/W for 30 μm bond-line thickness and 0.56 ± 0.10 mm^2 K/W for 50 μm bond-line thickness (please see the Supporting Information for more details) under adhesive load (i.e., no external load is applied). In both cases, the thermal contact resistance at the Si–TIM interface was 0.10 ± 0.03 mm^2 K/W as opposed 0.15 ± 0.04 mm^2 K/W for Si–Cu interface. We attributed this difference to the alleviation of interfacial mismatch between Si and Cu due to the presence of ligand molecules. The thermal resistance values contain the contribution from several interfaces and solid layers but are still very low compared with the traditional TIMs—at least a factor of 5 lower at comparable bond-line thicknesses.[22]

In general, the total thermal resistivity of a TIM strongly depends on its bulk thermal conductivity and Young's modulus, design parameters such as thickness and applied load (or adhesion force), and contact resistance. An ideal TIM should be both highly thermally conductive and mechanically compliant to effectively transport heat between two mating surfaces, and to be reliable. Hence, to put the measured properties of the hybrid nanocomposites into perspective, we relied on a bulk thermal conductivity versus Young's modulus plot and compared our values with the current-state-of-art and common TIMs (Figure 4). While the bulk thermal conductivity of the hybrid TIM was only 40% lower than that of pure copper (the base matrix), the compliance of the hybrid TIM was about 4 times larger than that of pure copper. In comparison to polymer TIMs, the hybrid nanocomposite TIMs lead to 1–2 orders of magnitude increase in the thermal conductivity with only a small loss in softness. The developed TIMs thermally outperform solder TIMs about 3–5-fold while they a slightly better mechanical compliance than solder TIMs.

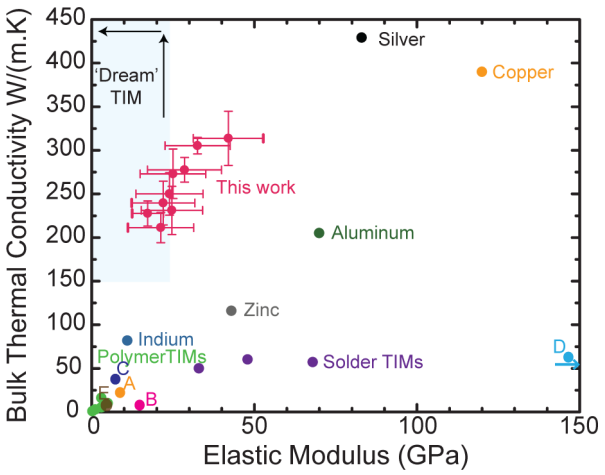

Figure 4. Comparison of bulk thermal conductivity versus elastic modulus values for various types of commonly used engineering thermal management materials, novel thermal management materials described in the literature (A,[33] B,[52] C,[53] D,[54] E[55]), and the developed chemically integrated metal/organic/inorganic nanocomposite thermal interface materials.

4. CONCLUSIONS

First, this work details a versatile and scalable approach based on chemisorption-coupled electrodeposition for producing chemically integrated/linked metal–organic–inorganic nanocomposites with a metal base matrix. Second, it demonstrates the proof-of-concept that 2-D boron nitride nanosheets (BNNS) can be functionalized with thiosemicarbazide (i.e., organic linker), which can bridge the metal matrix and BNNS. Third, hybrid nanomaterials developed through this approach display exceptional thermal and mechanical properties needed in thermal interface materials: Bulk thermal conductivities ranged from 211 to 277 W/(m K), which are very high considering their relatively low elastic modulus values on the order of 21.2–28.5 GPa. Overall, the chemically integrated metal/organic/inorganic hybrid nanocomposites provide a promising thermal management solution that can significantly reduce the thermal resistance in applications with high heat dissipation and can help in achieving the broader goals of compact, high-power-density (electronic) components.

■ ASSOCIATED CONTENT

Supporting Information

The Supporting Information is available free of charge on the ACS Publications website at DOI: 10.1021/acsami.7b00093.

Extended methods; synthesis and characterization of the BNNS and f-BNNS; and characterization and performance evaluation of TIMs (PDF)

Video on performance of the TIM materials (AVI)

■ AUTHOR INFORMATION

Corresponding Author

*E-mail makbulut@tamu.edu (M.A.).

ORCID

Mustafa Akbulut: 0000-0001-7343-2187

Author Contributions

C.Y. and N.N. contributed equally. C.Y. and N.N. performed the functionalization and thermal and mechanical characterization experiments, nanofabricated all the samples, analyzed

DOI: 10.1021/acsami.7b00093
ACS Appl. Mater. Interfaces XXXX, XXX, XXX–XXX

the data, and wrote the manuscript with significant input from M.A, S.N., T.C., and K.M. J.K.O. carried out FTIR measurements. The laser reflection studies were conducted by X.F. and C.K. in consultation with S.N. All SIMS measurements were done and analyzed by S.V. M.C. conducted high-resolution TEM experiments under the supervision of M.J.K. Raman spectroscopy measurements were performed by A.J.T. under the guidance of A.V.S. M.A. supervised this work. All authors discussed the results and reviewed the manuscript.

Notes

The authors declare no competing financial interest.

■ ACKNOWLEDGMENTS

This research was developed with funding from the Defense Advanced Research Projects Agency (DARPA, Award No. D13AP00040 to the Texas A&M University and IAG-12-1844 to NREL). The views, opinions, and/or findings expressed are those of the authors and should not be interpreted as representing the official views or policies of the Department of Defense or the U.S. Government. M.A. acknowledges funding from NSF Grant 1559627. A.T. and A.V.S. thank the Welch Foundation (Award No. A-1547) for support. A.J.T. and A.V.S. acknowledge funding from NSF (Grants PHY-1307153 and CHE-1609608) and thank the Welch Foundation (Award No. A-1547) for support.

■ ABBREVIATIONS

TIM, thermal interface material; CTE, coefficient of thermal expansion; BNNS, boron nitride nanosheets; TSC, thiosemicarbazide; MAS, magic-angle spinning; NMR, nuclear magnetic spectroscopy; TEM, transmission electron microscopy; XPS, X-ray photospectrometry; f-BNNS, functionalized boron nitride nanosheets; SEM, scanning electron microscopy; NMP, *N*-methlyl-2-pyrrolidone; PSTTR, phase-sensitive transient thermoreflectance.

■ REFERENCES

(1) Ghosh, S.; Calizo, I.; Teweldebrhan, D.; Pokatilov, E. P.; Nika, D. L.; Balandin, A. A.; Bao, W.; Miao, F.; Lau, C. N. Extremely High Thermal Conductivity of Graphene: Prospects for Thermal Management Applications in Nanoelectronic Circuits. *Appl. Phys. Lett.* **2008**, *92*, 151911.

(2) Zhang, Y.; Dembla, A.; Bakir, M. S. Silicon Micropin-Fin Heat Sink with Integrated TSVs for 3-D ICs: Tradeoff Analysis and Experimental Testing. *IEEE Trans. Compon., Packag., Manuf. Technol.* **2013**, *3*, 1842−1850.

(3) Wang, S.; Cheng, Y.; Wang, R.; Sun, J.; Gao, L. Highly Thermal Conductive Copper Nanowire Composites with Ultralow Loading: Toward Applications as Thermal Interface Materials. *ACS Appl. Mater. Interfaces* **2014**, *6*, 6481−6486.

(4) Barako, M. T.; Roy-Panzer, S.; English, T. S.; Kodama, T.; Asheghi, M.; Kenny, T. W.; Goodson, K. E. Thermal Conduction in Vertically Aligned Copper Nanowire Arrays and Composites. *ACS Appl. Mater. Interfaces* **2015**, *7*, 19251−19259.

(5) Swartz, E. T.; Pohl, R. O. Thermal Boundary Resistance. *Rev. Mod. Phys.* **1989**, *61*, 605−668.

(6) Pernot, G.; Stoffel, M.; Savic, I.; Pezzoli, F.; Chen, P.; Savelli, G.; Jacquot, A.; Schumann, J.; Denker, U.; Mönch, I.; Deneke, Ch.; Schmidt, O. G.; Rampnoux, J. M.; Wang, S.; Plissonnier, M.; Rastelli, A.; Dilhaire, S.; Mingo, N. Precise Control of Thermal Conductivity at the Nanoscale through Individual Phonon-Scattering Barriers. *Nat. Mater.* **2010**, *9*, 491−495.

(7) Prasher, R. Thermal Interface Materials: Historical Perspective, Status, and Future Directions. *Proc. IEEE* **2006**, *94*, 1571−1586.

(8) Yu, A.; Ramesh, P.; Sun, X.; Bekyarova, E.; Itkis, M. E.; Haddon, R. C. Enhanced Thermal Conductivity in a Hybrid Graphite Nanoplatelet - Carbon Nanotube Filler for Epoxy Composites. *Adv. Mater.* **2008**, *20*, 4740−4744.

(9) Wang, X.; Hu, Y.; Song, L.; Yang, H.; Xing, W.; Lu, H. In Situ Polymerization of Graphene Nanosheets and Polyurethane with Enhanced Mechanical and Thermal Properties. *J. Mater. Chem.* **2011**, *21*, 4222−4227.

(10) Stankovich, S.; Dikin, D. A.; Dommett, G. H. B.; Kohlhaas, K. M.; Zimney, E. J.; Stach, E. A.; Piner, R. D.; Nguyen, S. T.; Ruoff, R. S. Graphene-Based Composite Materials. *Nature* **2006**, *442*, 282−286.

(11) Biercuk, M. J.; Llaguno, M. C.; Radosavljevic, M.; Hyun, J. K.; Johnson, A. T.; Fischer, J. E. Carbon Nanotube Composites for Thermal Management. *Appl. Phys. Lett.* **2002**, *80*, 2767−2769.

(12) Jiang, H.; Moon, K.; Li, Y.; Wong, C. P. Surface Functionalized Silver Nanoparticles for Ultrahigh Conductive Polymer Composites. *Chem. Mater.* **2006**, *18*, 2969−2973.

(13) Yu, H.; Li, L.; Zhang, Y. Silver Nanoparticle-Based Thermal Interface Materials with Ultra-Low Thermal Resistance for Power Electronics Applications. *Scr. Mater.* **2012**, *66*, 931−934.

(14) Warzoha, R. J.; Zhang, D.; Feng, G.; Fleischer, A. S. Engineering Interfaces in Carbon Nanostructured Mats for the Creation of Energy Efficient Thermal Interface Materials. *Carbon* **2013**, *61*, 441−457.

(15) Chen, H.; Chen, M.; Di, J.; Xu, G.; Li, H.; Li, Q. Architecting Three-Dimensional Networks in Carbon Nanotube Buckypapers for Thermal Interface Materials. *J. Phys. Chem. C* **2012**, *116*, 3903−3909.

(16) Jung, H.; Yu, S.; Bae, N.-S.; Cho, S. M.; Kim, R. H.; Cho, S. H.; Hwang, I.; Jeong, B.; Ryu, J. S.; Hwang, J. High through-Plane Thermal Conduction of Graphene Nanoflake Filled Polymer Composites Melt-Processed in an L-Shape Kinked Tube. *ACS Appl. Mater. Interfaces* **2015**, *7*, 15256−15262.

(17) Park, J. S.; An, Y. J.; Shin, K.; Han, J. H.; Lee, C. S. Enhanced Thermal Conductivity of Epoxy/three-Dimensional Carbon Hybrid Filler Composites for Effective Heat Dissipation. *RSC Adv.* **2015**, *5*, 46989−46996.

(18) Lian, G.; Tuan, C.-C.; Li, L.; Jiao, S.; Wang, Q.; Moon, K.-S.; Cui, D.; Wong, C.-P. Vertically Aligned and Interconnected Graphene Networks for High Thermal Conductivity of Epoxy Composites with Ultralow Loading. *Chem. Mater.* **2016**, *28*, 6096−6104.

(19) Chung, D. D. L. Thermal Interface Materials. *J. Mater. Eng. Perform.* **2001**, *10*, 56−59.

(20) Roy, C. K.; Bhavnani, S.; Hamilton, M.; Johnson, W. R.; Knight, R. W.; Harris, D. K. Performance of Low Melt Alloys as Thermal Interface Materials. In *Thermal Measurement, Modeling & Management Symposium (SEMI-THERM), 2015 31st*; IEEE: 2015; pp 235−239.

(21) White, G. K. Thermal Expansion of Reference Materials: Copper, Silica and Silicon. *J. Phys. D: Appl. Phys.* **1973**, *6*, 2070.

(22) Bar-Cohen, A.; Matin, K.; Narumanchi, S. Nanothermal Interface Materials: Technology Review and Recent Results. *J. Electron. Packag.* **2015**, *137*, 040803.

(23) Panasonic. Pyrolytic Graphite Sheet.

(24) Minerals Technologies International (MTI), Inc. High Performance Pyrolytic Graphite Composite Heat Spreaders.

(25) Balandin, A. A. Thermal Properties of Graphene and Nanostructured Carbon Materials. *Nat. Mater.* **2011**, *10*, 569−581.

(26) Yan, Z.; Liu, G.; Khan, J. M.; Balandin, A. A. Graphene Quilts for Thermal Management of High-Power GaN Transistors. *Nat. Commun.* **2012**, *3*, 827.

(27) Leong, C. K.; Aoyagi, Y.; Chung, D. D. L. Carbon Black Pastes as Coatings for Improving Thermal Gap-Filling Materials. *Carbon* **2006**, *44*, 435−440.

(28) Zhi, C.; Bando, Y.; Tang, C.; Golberg, D. Boron Nitride Nanotubes. *Mater. Sci. Eng., R* **2010**, *70*, 92−111.

(29) Lin, Y.; Connell, J. W. Advances in 2D Boron Nitride Nanostructures: Nanosheets, Nanoribbons, Nanomeshes, and Hybrids with Graphene. *Nanoscale* **2012**, *4*, 6908.

(30) Lindsay, L.; Broido, D. A. Enhanced Thermal Conductivity and Isotope Effect in Single-Layer Hexagonal Boron Nitride. *Phys. Rev. B: Condens. Matter Mater. Phys.* **2011**, *84*, 1−6.

DOI: 10.1021/acsami.7b00093
ACS Appl. Mater. Interfaces XXXX, XXX, XXX−XXX

(31) Pham, T.; Goldstein, A. P.; Lewicki, J. P.; Kucheyev, S. O.; Wang, C.; Russell, T. P.; Worsley, M. A.; Woo, L.; Mickelson, W.; Zettl, A. Nanoscale Structure and Superhydrophobicity of sp2-Bonded Boron Nitride Aerogels. *Nanoscale* **2015**, *7*, 10449−10458.
(32) Sun, S.; Chen, S.; Luo, X.; Fu, Y.; Ye, L.; Liu, J. Mechanical and Thermal Characterization of a Novel Nanocomposite Thermal Interface Material for Electronic Packaging. *Microelectron. Reliab.* **2016**, *56*, 129−135.
(33) Zandén, C.; Luo, X.; Ye, L.; Liu, J. A New Solder Matrix Nano Polymer Composite for Thermal Management Applications. *Compos. Sci. Technol.* **2014**, *94*, 54−61.
(34) Luo, X.; Zhang, Y.; Zandén, C.; Murugesan, M.; Cao, Y.; Ye, L.; Liu, J. Novel Thermal Interface Materials: Boron Nitride Nanofiber and Indium Composites for Electronics Heat Dissipation Applications. *J. Mater. Sci.: Mater. Electron.* **2014**, *25*, 2333−2338.
(35) Murugesan, M.; Zandén, C.; Luo, X.; Ye, L.; Jokubavicius, V.; Syväjärvi, M.; Liu, J. A Carbon Fiber Solder Matrix Composite for Thermal Management of Microelectronic Devices. *J. Mater. Chem. C* **2014**, *2*, 7184.
(36) Oliver, W. C.; Pharr, G. M. An Improved Technique for Determining Hardness and Elastic Modulus Using Load and Displacement Sensing Indentation Experiments. *J. Mater. Res.* **1992**, *7*, 1564−1583.
(37) Losego, M. D.; Grady, M. E.; Sottos, N. R.; Cahill, D. G.; Braun, P. V. Effects of Chemical Bonding on Heat Transport across Interfaces. *Nat. Mater.* **2012**, *11*, 502−506.
(38) O'Brien, P. J.; Shenogin, S.; Liu, J.; Chow, P. K.; Laurencin, D.; Mutin, P. H.; Yamaguchi, M.; Keblinski, P.; Ramanath, G. Bonding-Induced Thermal Conductance Enhancement at Inorganic Heterointerfaces Using Nanomolecular Monolayers. *Nat. Mater.* **2012**, *12*, 118−122.
(39) Phelan, P. E.; Niemann, R. C. Effective Thermal Conductivity of a Thin, Randomly Oriented Composite Material. *J. Heat Transfer* **1998**, *120*, 971.
(40) Jo, I.; Pettes, M. T.; Kim, J.; Watanabe, K.; Taniguchi, T.; Yao, Z.; Shi, L. Thermal Conductivity and Phonon Transport in Suspended Few-Layer Hexagonal Boron Nitride. *Nano Lett.* **2013**, *13*, 550−554.
(41) Lin, W.; Moon, K.-S.; Wong, C. P. A Combined Process of in Situ Functionalization and Microwave Treatment to Achieve Ultrasmall Thermal Expansion of Aligned Carbon Nanotube-Polymer Nanocomposites: Toward Applications as Thermal Interface Materials. *Adv. Mater.* **2009**, *21*, 2421−2424.
(42) Xu, Y.; Chung, D. D. L.; Mroz, C. Thermally Conducting Aluminum Nitride Polymer-Matrix Composites. *Composites, Part A* **2001**, *32*, 1749−1757.
(43) Abtew, M.; Selvaduray, G. Lead-Free Solders in Microelectronics. *Mater. Sci. Eng., R* **2000**, *27*, 95−141.
(44) Min, Y.; Akbulut, M.; Kristiansen, K.; Golan, Y.; Israelachvili, J. The Role of Interparticle and External Forces in Nanoparticle Assembly. *Nat. Mater.* **2008**, *7*, 527−538.
(45) Halpin, J. C.; Kardos, J. L. The Halpin-Tsai Equations: A Review. *Polym. Eng. Sci.* **1976**, *16*, 344−352.
(46) Rafiee, M. A.; Rafiee, J.; Wang, Z.; Song, H.; Yu, Z. Z.; Koratkar, N. Enhanced Mechanical Properties of Nanocomposites at Low Graphene Content. *ACS Nano* **2009**, *3*, 3884−3890.
(47) Li, Y.; Jia, W. Z.; Song, Y. Y.; Xia, X. H. Superhydrophobicity of 3D Porous Copper Films Prepared Using the Hydrogen Bubble Dynamic Template. *Chem. Mater.* **2007**, *19*, 5758−5764.
(48) Mohan, S.; Raj, V. The Effect of Additives on the Electrodeposition of Copper. *Trans. Inst. Met. Finish.* **2005**, *83*, 194−198.
(49) Mammeri, F.; Le Bourhis, E.; Rozes, L.; Sanchez, C. Mechanical Properties of Hybrid Organic-Inorganic Materials. *J. Mater. Chem.* **2005**, *15*, 3787−3811.
(50) Li, C.; Bando, Y.; Zhi, C.; Huang, Y.; Golberg, D. Thickness-Dependent Bending Modulus of Hexagonal Boron Nitride Nanosheets. *Nanotechnology* **2009**, *20*, 385707.
(51) Kudin, K. N.; Scuseria, G. E.; Yakobson, B. I. C_2F, BN, and C Nanoshell Elasticity from Ab Initio Computations. *Phys. Rev. B: Condens. Matter Mater. Phys.* **2001**, *64*, 235406.
(52) Wong, C. P.; Bollampally, R. S. Thermal Conductivity, Elastic Modulus, and Coefficient of Thermal Expansion of Polymer Composites Filled with Ceramic Particles for Electronic Packaging. *J. Appl. Polym. Sci.* **1999**, *74*, 3396−3403.
(53) Xu, J.; Munari, A.; Dalton, E.; Mathewson, A.; Razeeb, K. M. Silver Nanowire Array-Polymer Composite as Thermal Interface Material. *J. Appl. Phys.* **2009**, *106*, 124310.
(54) Kuang, D.; Xu, L.; Liu, L.; Hu, W.; Wu, Y. Graphene-Nickel Composites. *Appl. Surf. Sci.* **2013**, *273*, 484−490.
(55) Jakubinek, M. B.; Ashrafi, B.; Guan, J.; Johnson, M. B.; White, M. A.; Simard, B. 3D Chemically Cross-Linked Single-Walled Carbon Nanotube Buckypapers. *RSC Adv.* **2014**, *4*, 57564−57573.

DOI: 10.1021/acsami.7b00093
ACS Appl. Mater. Interfaces XXXX, XXX, XXX−XXX